Temperature and tropopause characteristics from reanalyses data in the tropical tropopause layer

Susann Tegtmeier, James Anstey, Sean Davis, Rossana Dragani, Yayoi Harada, Ioana Ivanciu, Robin Pilch Kedzierski, Kirstin Krüger, Bernard Legras, Craig Long, et al.

Atmos. Chem. Phys., 20, 753–770, 2020
https://doi.org/10.5194/acp-20-753-2020

Atmospheric Chemistry and Physics
Open Access
EGU

Temperature and tropopause characteristics from reanalyses data in the tropical tropopause layer

Susann Tegtmeier[1,a], James Anstey[2], Sean Davis[3], Rossana Dragani[4], Yayoi Harada[5], Ioana Ivanciu[1], Robin Pilch Kedzierski[1], Kirstin Krüger[6], Bernard Legras[7], Craig Long[8], James S. Wang[9], Krzysztof Wargan[10,11], and Jonathon S. Wright[12]

[1]GEOMAR Helmholtz Centre for Ocean Research Kiel, 24105 Kiel, Germany
[2]Canadian Centre for Climate Modelling and Analysis, ECCC, Victoria, Canada
[3]Earth System Research Laboratory, National Oceanic and Atmospheric Administration, Boulder, CO 80305, USA
[4]European Centre for Medium-Range Weather Forecasts, Reading, RG2 9AX, UK
[5]Japan Meteorological Agency, Tokyo, 100-8122, Japan
[6]Section for Meteorology and Oceanography, Department of Geosciences, University of Oslo, 0315 Oslo, Norway
[7]Laboratoire de Météorologie Dynamique, CNRS/(PSL-ENS, Sorbonne Université, Ecole Polytechnique), Paris, France
[8]Climate Prediction Center, National Centers for Environmental Prediction, National Oceanic and Atmospheric Administration, College Park, MD 20740, USA
[9]Institute for Advanced Sustainability Studies, Potsdam, Germany
[10]Science Systems and Applications, Inc., Lanham, MD 20706, USA
[11]Global Modeling and Assimilation Office, Code 610.1, NASA Goddard Space Flight Center, Greenbelt, MD 20771, USA
[12]Department of Earth System Science, Tsinghua University, Beijing, 100084, China
[a]now at: Institute of Space and Atmospheric Studies, University of Saskatchewan, Saskatoon, Canada

Correspondence: Susann Tegtmeier (susann.tegtmeier@usask.ca)

Received: 18 June 2019 – Discussion started: 4 July 2019
Revised: 24 October 2019 – Accepted: 30 October 2019 – Published: 22 January 2020

Abstract. The tropical tropopause layer (TTL) is the transition region between the well-mixed convective troposphere and the radiatively controlled stratosphere with air masses showing chemical and dynamical properties of both regions. The representation of the TTL in meteorological reanalysis data sets is important for studying the complex interactions of circulation, convection, trace gases, clouds, and radiation. In this paper, we present the evaluation of climatological and long-term TTL temperature and tropopause characteristics in the reanalysis data sets ERA-Interim, ERA5, JRA-25, JRA-55, MERRA, MERRA-2, NCEP-NCAR (R1), and CFSR. The evaluation has been performed as part of the SPARC (Stratosphere–troposphere Processes and their Role in Climate) Reanalysis Intercomparison Project (S-RIP).

The most recent atmospheric reanalysis data sets (ERA-Interim, ERA5, JRA-55, MERRA-2, and CFSR) all provide realistic representations of the major characteristics of the temperature structure within the TTL. There is good agreement between reanalysis estimates of tropical mean temperatures and radio occultation data, with relatively small cold biases for most data sets. Temperatures at the cold point and lapse rate tropopause levels, on the other hand, show warm biases in reanalyses when compared to observations. This tropopause-level warm bias is related to the vertical resolution of the reanalysis data, with the smallest bias found for data sets with the highest vertical resolution around the tropopause. Differences in the cold point temperature maximize over equatorial Africa, related to Kelvin wave activity and associated disturbances in TTL temperatures.

Interannual variability in reanalysis temperatures is best constrained in the upper TTL, with larger differences at levels below the cold point. The reanalyses reproduce the temperature responses to major dynamical and radiative signals such as volcanic eruptions and the quasi-biennial oscillation (QBO). Long-term reanalysis trends in temperature in the upper TTL show good agreement with trends derived from

adjusted radiosonde data sets indicating significant stratospheric cooling of around -0.5 to -1 K per decade. At 100 hPa and the cold point, most of the reanalyses suggest small but significant cooling trends of -0.3 to -0.6 K per decade that are statistically consistent with trends based on the adjusted radiosonde data sets.

Advances of the reanalysis and observational systems over the last decades have led to a clear improvement in the TTL reanalysis products over time. Biases of the temperature profiles and differences in interannual variability clearly decreased in 2006, when densely sampled radio occultation data started being assimilated by the reanalyses. While there is an overall good agreement, different reanalyses offer different advantages in the TTL such as realistic profile and cold point temperature, continuous time series, or a realistic representation of signals of interannual variability. Their use in model simulations and in comparisons with climate model output should be tailored to their specific strengths and weaknesses.

1 Introduction

The tropical tropopause layer (TTL) is the transition region between the well-mixed convective troposphere and the radiatively controlled stratosphere. The vertical range of the TTL extends from the region of strong convective outflow near 12–14 km to the highest altitudes reached by convective overshooting events, around 18 km (Highwood and Hoskins, 1998; Folkins et al., 1999; Fueglistaler et al., 2009; Randel and Jensen, 2013). Air masses in the TTL show dynamical and chemical properties of both the troposphere and the stratosphere and are controlled by numerous processes on a wide range of length and timescales. Complex interactions among circulation, convection, trace gases, clouds, and radiation in the TTL make this region a key player in radiative forcing and chemistry–climate coupling. As the TTL is the main gateway for air entering the stratosphere, chemistry and composition of the stratosphere, and especially the abundances of ozone, water vapor, and aerosols, are strongly impacted by the properties of air near the tropical tropopause (e.g., Mote et al., 1996; Holton and Gettelman, 2001; Fueglistaler et al., 2011).

The tropopause is the most important physical boundary within the TTL, serving to separate the turbulent, moist troposphere from the stable, dry stratosphere. The position of the tropopause is determined by the thermal properties of the TTL, where the negative vertical temperature gradient of the troposphere changes into the positive temperature gradient of the stratosphere. The role of the tropopause as a physical boundary is evident not only from the vertical temperature structure but also from the distributions of atmospheric trace gases and clouds (Pan and Munchak, 2011; Pan et al., 2018).

In the tropics, two definitions of the tropopause are widely used: one based on the cold point and one based on the characteristics of the lapse rate. The cold point tropopause is defined as the level at which the vertical temperature profile reaches its minimum (Highwood and Hoskins, 1998) and air parcels en route from the troposphere to the stratosphere encounter the lowest temperatures. Final dehydration typically occurs at these lowest temperatures, so the cold point tropopause effectively controls the overall water vapor content of the lower stratosphere (Randel et al., 2004a) and explains its variability (Fueglistaler et al., 2009). While the cold point tropopause is an important boundary in the tropics where upwelling predominates, this definition of the tropopause is irrelevant for water vapor transport into the stratosphere at higher latitudes. The lapse rate tropopause, on the other hand, offers a globally applicable definition of the tropopause, marking a vertical discontinuity in the static stability. The lapse rate tropopause is defined as the lowest level at which the lapse rate decreases to $2\,\mathrm{K\,km^{-1}}$ or less, provided that the average lapse rate between this level and all higher levels within 2 km does not exceed $2\,\mathrm{K\,km^{-1}}$ (World Meteorological Organization, 1957). The tropical lapse rate tropopause is typically ~ 0.5 km (~ 7 hPa) lower and ~ 1 K warmer than the cold point tropopause (Seidel et al., 2001).

Over recent decades, the thermal characteristics of the TTL and tropopause have been obtained from tropical radiosonde and Global Navigation Satellite System – Radio Occultation (GNSS-RO) upper-air measurements. Radiosonde profiles offer temperature, wind, and air pressure data at a high vertical resolution. However, climate records based on radiosonde data often suffer from spatial inhomogeneities or time-varying biases due to changes in instruments and measurement practices (Seidel and Randel, 2006; Wang et al., 2012). Climate records from radio occultation data offer much better spatial coverage and density but are only available starting from 2002. As a result, studies of long-term variability and trends in TTL and tropopause properties have also used reanalysis data (e.g., Santer et al., 2003; Gettelman et al., 2010; Xie et al., 2014).

Meteorological reanalysis data sets are widely used in scientific studies of atmospheric processes and variability, either as initial conditions for historical model runs or in comparisons with climate model output. Often, they are utilized as "stand-ins" for observations, when the available measurements lack the spatial or temporal coverage needed. Each atmospheric reanalysis system consists of a fixed global forecast model and assimilation scheme. The system combines short-range forecasts of the atmospheric state with available observations to produce consistent best-guess estimates of atmospheric variables such as temperatures and winds. Spurious changes in the reanalysis fields can arise from changes in the quality and quantity of the observations used as input data, which complicates the analysis of variability and trends. Further discontinuities in reanalysis-based time se-

ries can originate from joining together distinct execution streams (Fujiwara et al., 2017).

Among the various TTL characteristics such as composition, radiation budgets, and cloud properties, the vertical temperature structure and the position and temperature of the cold point are of particular importance for transport and composition studies. Many offline chemical transport models or Lagrangian particle dispersion models are driven by reanalysis data sets (e.g., Chipperfield, 1999; Krüger et al., 2009; Schoeberl et al., 2012; Tao et al., 2019). Their representation of the cold point determines how realistically such models simulate dehydration and stratospheric entrainment processes. Process studies of TTL dynamics such as equatorial wave variability are also often based on the TTL temperature structure in reanalysis data sets (e.g., Fujiwara et al., 2012). Finally, reanalysis cold point temperature and height have been used in the past for comparison to model results and in investigations of long-term changes (e.g., Gettelman et al., 2010). Information on the quality and biases of TTL temperature and tropopause data is important for all above listed studies of transport, composition, dynamics, and long-term changes in the TTL.

A comparison of the reanalysis products available at the end of the 1990s (including ERA-15, ERA-40 and NCEP-NCAR R1) with other climatological data sets showed notable differences in temperatures near the tropical tropopause (Randel et al., 2004b). While the ECMWF reanalyses agreed relatively well with radiosonde observations at 100 hPa, NCEP-NCAR R1 showed a warm bias of up to 3 K, probably resulting from low vertical resolution and the use of poorly resolved satellite temperature retrievals (Fujiwara et al., 2017). Comparisons of winter temperatures at 100 hPa between more recent reanalyses, such as MERRA, NCEP CFSR, and ERA-Interim, and Singapore radiosonde observations show better agreement, with reanalyses generally 1–2 K too cold at this level (Schoeberl et al., 2012). While many studies have highlighted the characteristics of individual reanalysis data sets, a comprehensive intercomparison of the TTL among all major atmospheric reanalyses is currently missing.

Here, we investigate whether the reanalysis data sets ERA-Interim, ERA5, JRA-25, JRA-55, MERRA, MERRA-2, NCEP-NCAR (R1), and CFSR reproduce key characteristics of the temperature and tropopause levels in the TTL. This work has been conducted as part of the SPARC (Stratosphere–troposphere Processes and their Role in Climate) Reanalysis Intercomparison Project (S-RIP) (Fujiwara et al., 2017) and presents some of the key findings from the S-RIP report Chapter 8 on the TTL. Climatologies of the tropical cold point and lapse rate tropopause levels as derived from modern reanalysis data sets are compared to high-resolution radio occultation data (Sect. 3). We also investigate temporal variability and long-term changes in tropopause levels and temperature within the TTL (Sect. 4). The observational and reanalysis data sets used in the evaluation are introduced in Sect. 2, and a discussion and summary of the results are provided in Sect. 5.

2 Data and methods

2.1 Observational data sets

Observations of the TTL temperatures are available from tropical radiosonde stations. However, climate records of radiosonde temperature, height, and pressure data often suffer from inhomogeneities or time-varying biases due to changes in instruments or measurement practices (Seidel and Randel, 2006). Adjusted radiosonde temperature data sets at 100 and 70 hPa and corresponding trends at the cold point have been created by removing such inhomogeneities (Wang et al., 2012, and references therein). In this section, we use the four independently adjusted radiosonde data sets RATPAC (Free et al., 2005), RAOBCORE (Haimberger, 2007), RICH (Haimberger et al., 2012), and HadAT (Thorne et al., 2005) for evaluations at 70 and 100 hPa. The interannual anomalies at 70 hPa are shown only for RAOBCORE to improve the clarity of the figure, but all data sets are discussed in the text. For trends at 70 and 100 hPa, we show the smallest and largest trends derived from the four adjusted radiosonde data sets as reported by Wang et al. (2012) and consider their range (including error bars) as the observational uncertainty range.

Evaluations of the interannual anomalies of cold point temperature, height, and pressure are based on the unadjusted quality-controlled radiosonde data set IGRA (Durre et al., 2006) as temperature adjustments can change the location of the cold point in a profile. The trend of cold point temperature cannot be derived from the unadjusted IGRA data set due to inhomogeneities or time-varying biases caused by changes in instruments and measurement practices (see Wang et al., 2012 for a detailed discussion). Instead we use adjusted cold point trends derived from the adjusted radiosonde data sets discussed above.

Since 2002, high-resolution temperature and pressure data in the TTL are also available from satellite retrievals based on the GNSS-RO technique. Recent studies have demonstrated good agreement between GNSS-RO and radiosonde temperature profiles (e.g., Anthes et al., 2008; Ho et al., 2017). We use a monthly mean zonal mean data set constructed from measurements collected by the CHAllenging Minisatellite Payload (CHAMP; Wickert et al., 2001), Gravity Recovery and Climate Experiment (GRACE; Beyerle et al., 2005), Constellation Observing System for Meteorology, Ionosphere, and Climate (COSMIC; Anthes et al., 2008), Metop-A (von Engeln et al., 2011), Metop-B, Satélite de Aplicaciones Científicas-C/Scientific Application Satellite-C (SAC-C; Hajj et al., 2004), and TerraSAR-X (Beyerle et al., 2011) missions. All data are reprocessed or post-processed occultation profiles with moisture information ("wetPrf"

product) as provided by the COSMIC Data Analysis and Archive Center (CDAAC, https://cdaac-www.cosmic.ucar.edu/cdaac/products.html, last access: January 2019). The GNSS-RO "wetPrf" temperature profiles from CDAAC are provided on a 100 m vertical grid from the surface to 40 km altitude. The effective physical resolution is variable, ranging from $\sim$ 1 km in regions of constant stratification down to 100–200 m where the biggest stratification gradients occur, e.g., at the top of the boundary layer or at a very sharp tropopause (Kursinski et al., 1997; Gorbunov et al., 2004), most often being somewhere in between. The observational temperature records at reanalysis model levels in the TTL region have been determined by interpolating each GNSS-RO temperature profile to the reanalysis model levels with the barometric formula, taking into account the lapse rate between levels. For each profile, the cold point and lapse rate tropopause characteristics were identified based on the cold point and World Meteorological Organization (WMO) criteria, respectively. Zonal and long-term averages of the tropopause metrics and temperatures at model levels are calculated by averaging over all grid points and represent the final step of data processing.

We also use a daily data set of cold point temperatures obtained from all GNSS-RO missions, gridded on a $5^\circ \times 5^\circ$ grid between 30° N and 30° S. For each 5° wide latitude band, we apply a two-dimensional fast Fourier transform to detect Kelvin wave anomalies for planetary wavenumbers 1–15, periods of 4–30 d, and equivalent depths of 6–600 following the theoretical dispersion curves for Kelvin waves as in Wheeler and Kiladis (1999). We allow a wider range of equivalent depths, since it has been shown that Kelvin waves tend to propagate faster around the tropical tropopause than they do in the troposphere (Kim and Son, 2012). The filtered anomalies represent cold point temperature variability that propagates in the same wavenumber–frequency domain as Kelvin waves, i.e., when the temperature is modulated by Kelvin waves present around the tropopause. The spatial variance of the filtered signals is used to calculate a monthly index as a measure of the amount of Kelvin wave activity in the TTL. The index is calculated as the 1σ standard deviation over the filtered anomalies at all spatial grid points. Time periods of enhanced Kelvin wave activity are defined as the months when the index is larger than the long-term mean plus the 1σ standard deviation of the whole time series. Based on this definition, we determined 20 % of all months to be characterized by enhanced Kelvin wave activity.

2.2 Reanalysis data sets

We evaluate eight "full-input" reanalyses, where a full-input reanalysis is defined as a system that assimilates surface and upper-air conventional and satellite data. In this paper, we focus on the European Centre for Medium-Range Weather Forecasts (ECMWF) Interim Reanalysis (ERA-Interim; Dee et al., 2011), the forthcoming reanalysis developed by ECMWF (ERA5; Hersbach et al., 2018), the Japanese 25-year Reanalysis (JRA-25; Onogi et al., 2007), the Japanese 55-year Reanalysis (JRA-55; Kobayashi et al., 2015), the Modern Era Retrospective-Analysis for Research and Applications (MERRA; Rienecker et al., 2011), the MERRA-2 (Gelaro et al., 2017), the National Centers for Environmental Prediction (NCEP) – National Center for Atmospheric Research (NCAR) Reanalysis 1 (NCEP-NCAR Reanalysis 1; Kistler et al., 2001; referred to hereafter as R1), and the NCEP Climate Forecast System Reanalysis (CFSR; Saha et al., 2010). We limit our analyses to the S-RIP core intercomparison period 1980–2010. Due to availability at the time of the evaluations, ERA5 is only evaluated over 2002–2010. Details of each reanalysis, including model characteristics, physical parameterizations, assimilated observations, execution streams, and assimilation strategies have been summarized by Fujiwara et al. (2017).

Global temperature fields in the reanalysis data sets are constrained by assimilating conventional (surface and balloon), aircraft, and satellite observations. The most important sources of assimilated data for stratospheric temperatures are the microwave and infrared satellite sounders of the TOVS suite (1979–2006) and the ATOVS suite (1998–present). All of the above reanalysis systems assimilate microwave and infrared radiance from these instruments, except for NCEP-NCAR R1 which assimilates temperature retrievals instead. Measurements from the ATOVS suite, which has a higher number of channels compared to TOVS, have been assimilated from about 1998, although the exact start dates differ among the reanalyses. The introduction of ATOVS considerably improved the vertical resolution of the assimilated data. Some of the reanalyses (ERA-Interim, ERA5, MERRA, MERRA-2, and CFSR) also assimilate radiance estimates from the hyperspectral infrared sounders AIRS (2002–present), IASI (2008–present), and/or CrIS (2012–present), although the latter was not available for assimilation during the intercomparison period considered here. Because radiance biases associated with instrument changes, inaccurate calibration offsets, orbital drifts, or long-term CO_2 changes can cause unwanted biases in the resulting reanalysis temperature fields (e.g., Rienecker et al., 2011), a variational bias correction scheme is used during the data assimilation procedure to remove or minimize any radiance biases. This ensures that any temperature changes introduced by the circumstances outlined above are kept small, which is important when looking for long-term changes.

All full-input reanalyses assimilate upper-air temperature observations from radiosondes, which are available at a very high vertical resolution. Systematic errors in radiosonde profiles caused by effects of solar radiative heating on the temperature sensor (Nash et al., 2011) have typically been corrected either on-site or at the reanalysis center before assimilation (Fujiwara et al., 2017). In order to avoid discontinuities or inconsistencies in temperature time series from radiosondes, several reanalysis systems use homogenized tempera-

Table 1. List of GNSS-RO data assimilated by the reanalysis systems with starting dates prior to the end of 2010.

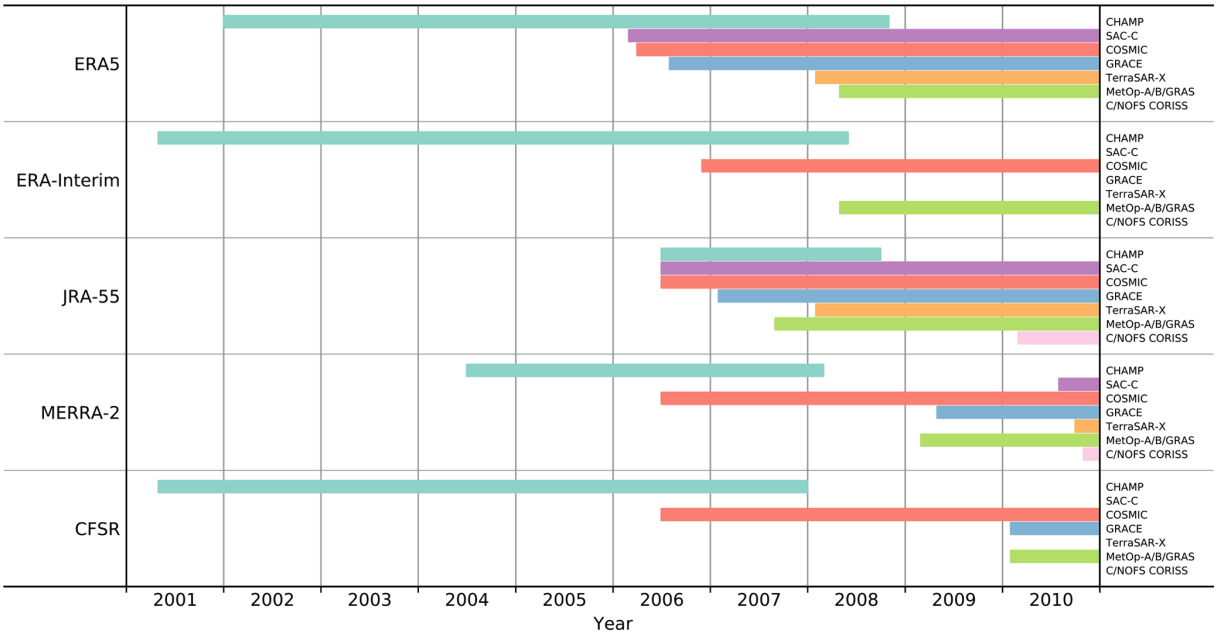

ture data sets such as RAOBCORE (ERA-Interim, JRA-55, MERRA, MERRA-2) and RICH (ERA5). Earlier reanalyses (ERA-40 and JRA-25) used simplified homogenization approaches that mostly corrected for daily and seasonal variations. Although the detailed quality-control procedures for radiosonde and other conventional data imported from the global distribution network can vary among the individual reanalyses, the conventional data archives are often shared among the centers (see also Fujiwara et al., 2017).

Recent reanalysis systems have also included information from GNSS-RO instruments by assimilating observations of the bending angle up to 30 km (Cucurull et al., 2013). Assimilating these high vertical resolution data affects reanalysis temperature and provides an additional "anchor" for adaptive bias correction of satellite radiance. JRA-55 assimilates refractivity profiles up to 30 km, which are functions of temperature, humidity, and pressure. For all recent reanalyses, the advent of the COSMIC mission in 2006 significantly increased the number of GNSS-RO profiles available for assimilation. Details of the various GNSS-RO data assimilated by ERA5, ERA-Interim, JRA-55, MERRA-2, and CFSR up to the end of 2010 are listed in Table 1. In addition to the GNSS-RO data sets discussed in Sect. 2.1, C/NOFS-CORISS (Communications/Navigation Outage Forecasting System Occultation Receiver for Ionospheric Sensing and Specification) is assimilated by some of the reanalyses.

Among the observational data sets, radiosonde and GNSS-RO data are our best source of information about the TTL. While the reanalyses assimilate different versions of these data, it is not certain that they reproduce the data within their uncertainty. For instance, discrepancies exist between reanalysis stratospheric temperatures and those derived from their radiance input data (Long et al., 2017). In fact, it is a subject of ongoing research how well reanalyses fit the data they assimilate (Simmons et al., 2014; Wright and Hindley, 2018). The data assimilation systems combine information from a model, a set of observations, and a priori information weighted by their respective uncertainties. The degraded vertical resolution of the reanalyses, compared to radiosonde and GNSS-RO data also leads to differences, especially for derived quantities such as the tropopause location and temperature, which will be investigated in the following evaluations.

The reanalysis models resolve the TTL with different vertical resolutions, as illustrated in Fig. 1. The number of model levels between 200 and 70 hPa varies among the reanalyses from a low of 4 (NCEP-NCAR R1) to a high of 21 (ERA5), corresponding to vertical resolutions between ~ 1.5 and ~ 0.2 km. In addition to the native model levels, all reanalyses provide post-processed data on standard pressure levels with at least four levels situated between 200 and 70 hPa (Fig. 1). The horizontal resolutions of the reanalysis products are approximately $0.25° \times 0.25°$ (ERA5), $0.7° \times 0.7°$ (ERA-Interim), $0.63° \times 0.5°$ (MERRA-2), $0.66° \times 0.5°$ (MERRA), $0.56° \times 0.56°$ (JRA-55), $1.13° \times 1.13°$ (JRA-25), $0.5° \times 0.5°$ (CFSR), and $1.9° \times 1.9°$ (R1).

2.3 Methods

Given the strong gradients of temperature and static stability in the TTL, the vertical resolution of the reanalysis data sets is an important factor in cold point and lapse rate tropopause calculations. For each reanalysis, tropopause

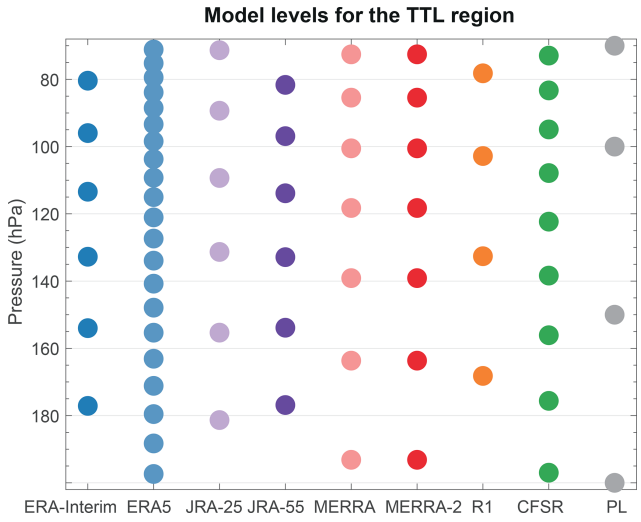

Figure 1. Model-level pressure values for different reanalysis data sets in the TTL using a fixed surface pressure of 1013.25 hPa. Standard pressure levels (PL) in the TTL region are also shown.

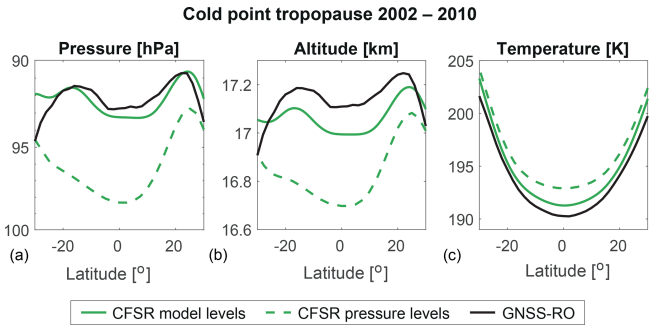

Figure 2. Latitudinal distributions of zonal-mean cold point tropopause pressure **(a)**, altitude **(b)**, and temperature **(c)** based on radio occultation data (black) and CFSR model-level (green solid) and pressure-level (green dashed) data during 2002–2010.

heights and temperatures can be derived either from model- or pressure-level data (Fig. 1). A comparison of the CFSR cold point tropopause based on model- and pressure-level temperature data is shown here to demonstrate the clear advantage of the finer model-level resolution (Fig. 2). The cold point tropopause from CFSR model-level data for the time period 2002–2010 agrees well with radio occultation results, with differences of less than 1.5 K and 0.2 km at all latitudes. The tropopause derived from CFSR pressure-level data, on the other hand, shows larger differences. This estimate is up to 0.4 km too low and up to 3 K too warm, illustrating the need to use data with high vertical resolution to identify and describe the tropopause. We derive the cold point and lapse rate tropopause characteristics for each reanalysis using model-level data between 500 and 10 hPa at each grid point at 6-hourly temporal resolution. Zonal and long-term averages are calculated by averaging over all grid points, and represent the final step of data processing. For our calculations, the cold point tropopause is defined as the coldest model level. The lapse rate tropopause is defined as the lowest level at which the lapse rate decreases to 2 K km^{-1} or less, provided that the average lapse rate between this level and all higher levels within 2 km does not exceed 2 K km^{-1} (World Meteorological Organization, 1957).

The evaluation of the interannual variability (Sect. 4) is based on time series of deseasonalized monthly temperature, pressure, and altitude anomalies calculated relative to the mean annual cycle during 2002–2010. To study variability driven by tropospheric and stratospheric forcing, we identify and isolate the variations based on a standard multivariate regression analysis:

$$T(t) = A_1 \cdot \mathrm{QBO1}(t) + A_2 \cdot \mathrm{QBO2}(t) + B \cdot \mathrm{ENSO}(t) + D \cdot \mathrm{VOL}(t). \quad (1)$$

Here QBO1 (t) and QBO2 (t) are orthogonal time series representing quasi-biennial oscillation (QBO) variations constructed as the first two empirical orthogonal functions (EOFs) of the Freie Universität Berlin (FUB) radiosonde stratospheric winds (Naujokat, 1986). ENSO (t) is the multivariate ENSO index (https://www.esrl.noaa.gov/psd/enso/mei/, last access: January 2019) and VOL (t) is the stratospheric aerosol optical depth from the Global Space-based Stratospheric Aerosol Climatology (Thomason et al., 2018). The standard error of the regression coefficients was derived based on the bootstrap method (Efron and Tibshirani, 1993). The QBO temperature amplitude is calculated as the difference between the averaged maxima and averaged minima values of the time series of the QBO temperature variations, $A_1 \cdot \mathrm{QBO1}(t) + A_2 \cdot \mathrm{QBO2}(t)$. For each QBO cycle of this time series, the absolute temperature maximum and minimum are selected. In a second step, the means over all such temperature maxima and minima are calculated to give the averaged maximum and minimum values, respectively.

The long-term trends of the reanalyses temperature time series have been derived as the regression coefficient of a linear function that provides the best fit in a least-squares sense. The uncertainty in each long-term trend is calculated as the standard error of the slope with the effective sample size adjusted to account for the corresponding lag-1 autocorrelation coefficient. Significance is tested based on a two-tailed test with a 95 % confidence interval.

3 Temperature and tropopause characteristics

Tropical mean temperatures from reanalyses at two standard pressure levels (100 and 70 hPa) and at the two tropopause levels are compared to radio occultation data for the time

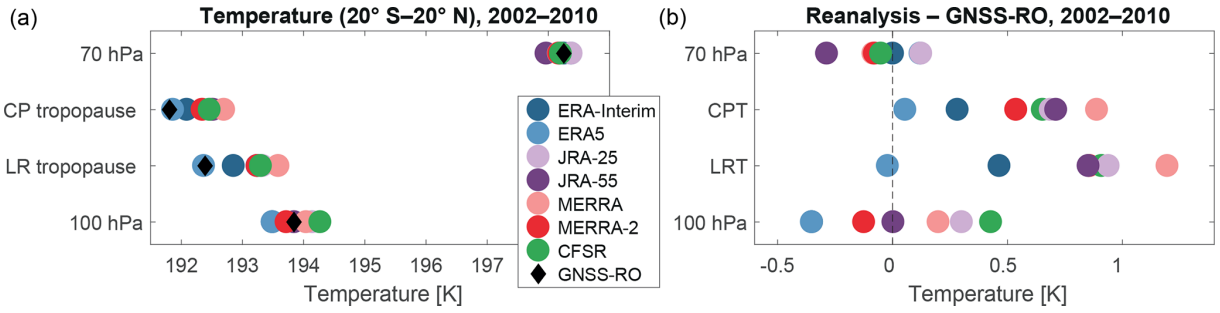

Figure 3. Tropical mean (20° S–20° N) temperatures at 100 hPa, the lapse rate tropopause (LRT), the cold point tropopause (CPT), and 70 hPa from reanalyses and GNSS-RO data during 2002–2010 **(a)**. Differences between the GNSS-RO and reanalysis temperatures are shown in panel **(b)**. At 100 hPa, ERA-Interim is hidden by ERA-5; at the LRT, MERRA-2 is hidden by JRA-55; and at 70 hPa, ERA5 is hidden by JRA-25 and MERRA is hidden by MERRA-2.

period 2002–2010 (Fig. 3). At 100 hPa, reanalysis temperatures agree well with radio occultation data with differences between −0.35 K (too cold; ERA-Interim and ERA5) and 0.43 K (too warm; CFSR). At 70 hPa, the agreement is even better, with differences ranging from −0.29 K (JRA-55) to 0.12 K (JRA-25). However, nearly all reanalyses show warm biases at both tropopause levels, with differences of up to 1.2 K compared to the observations. Most likely, the excess warmth of tropopause estimates based on reanalysis products stems from the limited vertical resolution of the reanalysis models in the TTL region. The best agreement is found for the reanalysis with the highest vertical resolution (ERA5; 0.05 K too warm at the cold point tropopause). The data set with the lowest vertical resolution (NCEP-NCAR R1) is 2.2 K too warm, outside the range displayed in Fig. 3.

Temperature profile comparisons between 140 and 70 hPa at the native model levels have been conducted for the five most recent reanalyses (ERA5, ERA-Interim, JRA-55, MERRA-2, CFSR). All reanalyses tend to be colder than the observations in the tropical mean (Fig. 4), but differences are relatively small and the agreement is good overall. CFSR and ERA5 agree best with the radio occultation data with mean biases of around −0.06 and −0.28 K, respectively, averaged over the whole vertical range. ERA-Interim and MERRA-2 agree very well at upper levels but show large deviations on model levels near 100 hPa (ERA-Interim; −0.82 K) and below 110 hPa (MERRA-2; −0.67 K), respectively. The evaluation demonstrates that temperature comparisons at standard pressure levels (Fig. 3) can be biased by up to 0.5 K, with CFSR showing a positive bias (0.45 K) at the 100 hPa standard pressure level but very good agreement (−0.05 K) at nearby native model levels. Such biases can result from vertical interpolation of temperature data in regions with large lapse rate changes.

Comparing the temperature profiles to the tropopause values (Figs. 3 and 4) reveals that despite the five reanalyses having negative biases at model levels, they mostly have positive biases at the cold point and lapse rate tropopause levels. As the discrete values corresponding to reanalysis model levels are unable to reproduce the true minimum temperature as recorded in a near-continuous profile, this difference can be expected for the cold point tropopause. Similarly, the lapse rate tropopause criteria might typically be fulfilled at lower levels for data at coarser resolution, thus resulting in a warm bias at the lapse rate tropopause on average. Overall, our results indicate that the negative temperature bias at model levels is more than canceled out by the positive bias introduced when calculating the cold point and lapse rate tropopause levels. Linking the temperature profile and tropopause comparisons, this "bias shift" is about 0.3 K for ERA5, 0.6 K for CFSR, and 1 K or larger for ERA-Interim, MERRA-2, and JRA-55. In consequence, ERA5, with both a small negative

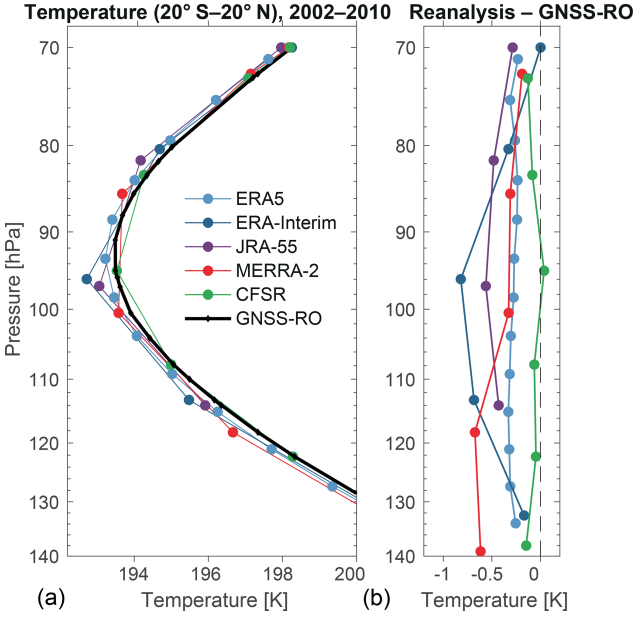

Figure 4. Tropical mean (20° S–20° N) temperature profiles at reanalysis model levels between 140 and 70 hPa **(a)** during 2002–2010 and differences between reanalysis and GNSS-RO temperatures **(b)**.

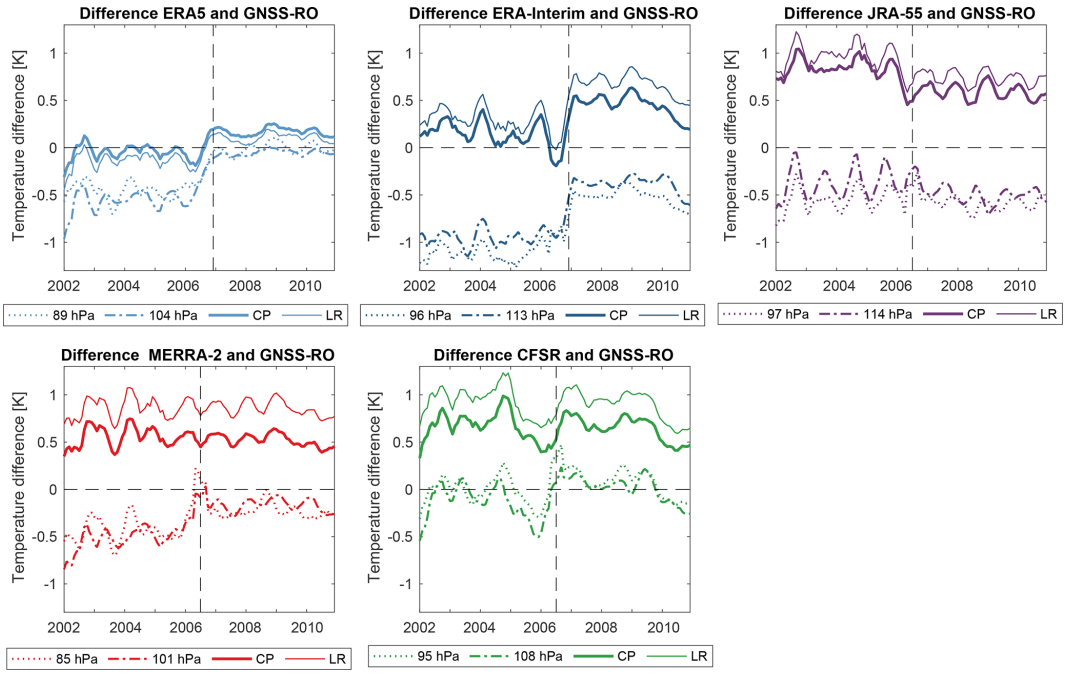

Figure 5. Tropical mean (20° S–20° N) time series of temperature differences between reanalysis and radio occultation at the cold point (CP) and lapse rate (LR) tropopause levels, as well as selected reanalysis model levels. Vertical lines indicate when the assimilation of COSMIC radio occultation data started.

bias at the model levels and a small bias shift, provides the most realistic tropopause temperatures. CFSR also has a relatively small bias shift, but the relatively unbiased temperature profile does not permit any error cancelation via this shift, so cold point and lapse rate tropopause levels based on CFSR are systematically too warm.

Agreement between the reanalysis temperature profiles and GNSS-RO data clearly improves when the comparison is restricted to the 2007–2010 time period, when the more densely sampled COSMIC data were assimilated (Table 1). This point is illustrated by comparison of temperature time series from reanalyses and observations at two model and both tropopause levels (Fig. 5). For ERA5, ERA-Interim, and MERRA-2, the cold bias with respect to GNSS-RO at model levels decreases after 2007, most likely because of the high number of daily COSMIC profiles available for assimilation from this time onwards. Cold biases at model levels are accompanied by warm biases in the tropopause temperatures, which, for ERA-Interim and ERA5, increase after 2007. As the increase at all levels is very similar, this indicates that the advantage of a reduced temperature bias at model levels comes at the expense of an increased temperature bias at the tropopause. CFSR and MERRA-2 show no such systematic change in their tropopause temperatures over time when compared to GNSS-RO data. JRA-55 is the only reanalysis product for which cold point and lapse rate tropopause temperatures agree slightly better with GNSS-RO estimates after 2007.

Evaluations of the latitudinal structure of the cold point tropopause for 2002–2010 are based on comparisons to radio occultation data (Fig. 6). All reanalysis data sets produce tropopause levels that are too low and too warm, with the latter related to vertical resolution as explained above. The observations show that average cold point temperatures are lowest right around the Equator. The reanalyses fail to reproduce this latitudinal gradient, indicating more constant cold point temperatures across the inner tropics between 10° S and 10° N with a less pronounced minimum at the Equator. As a consequence, the largest differences in cold point tropopause temperatures relative to GNSS-RO data are at the Equator and the best agreement is around 20° S–20° N for all reanalysis data sets.

The cold point altitude and pressure exhibit little north–south variability, ranging from 16.9 km (94 hPa) to 17.2 km (91.8 hPa). With respect to the seasonal cycle, it is well known that the temperature and altitude of the cold point tropopause are linked, with the coldest temperatures and highest altitudes observed during boreal winter (e.g., Seidel et al., 2001; Kim and Son, 2012). This relationship does not hold in the meridional direction: the highest cold point altitudes are located around 20° S–20° N, while the lowest cold point temperatures are located near the Equator. The higher altitude and lower pressure of the cold point tropopause around 20° S–20° N results from zonally variable features linked to tropospheric pressure regimes, such as particularly low tropopause pressures over the Tibetan

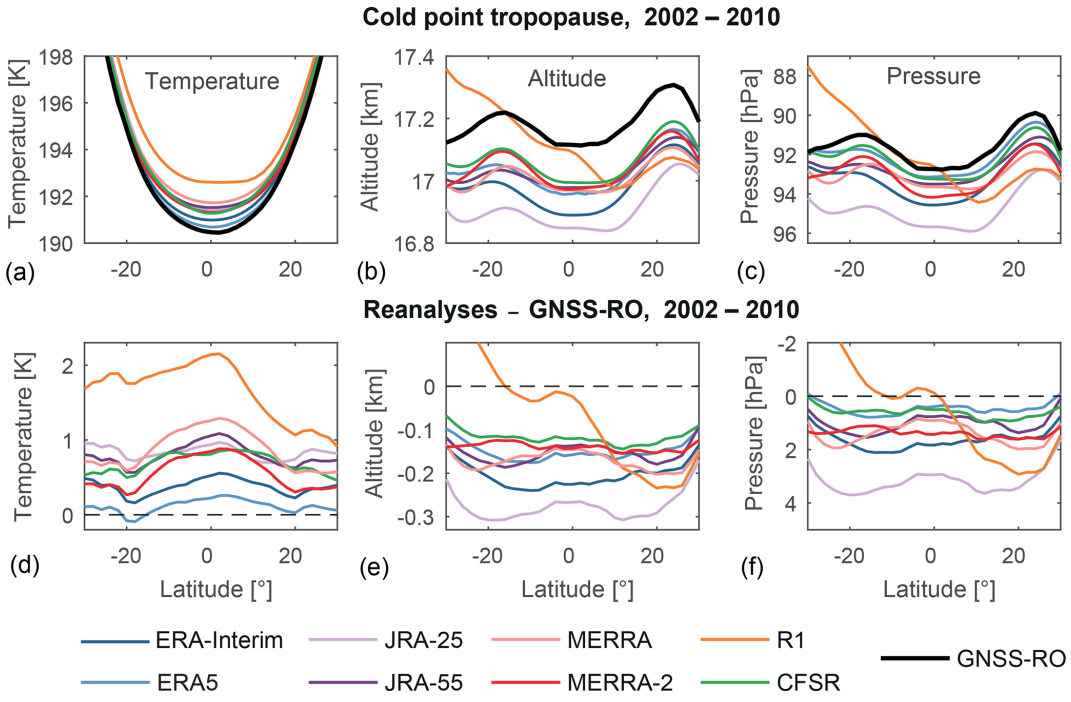

Figure 6. Latitudinal distributions of zonal-mean cold point tropopause temperature **(a)**, altitude **(b)**, and pressure **(c)** based on radio occultation data and reanalysis products during 2002–2010 **(a–c)**. Differences between radio occultation and reanalysis estimates are shown in panels **(d)**–**(f)**.

Plateau during boreal summer (Kim and Son, 2012). The reanalysis data sets capture most of this latitudinal structure, showing roughly constant differences between about 0.1 and 0.2 km (0–2 hPa). The largest differences are found for NCEP-NCAR R1 in the Southern Hemisphere, where the cold point tropopause based on R1 is both higher and warmer than observed. The best agreement with respect to cold point temperatures is found for ERA5 and ERA-Interim, which are around 0.2 and 0.4 K warmer than the radio occultation data, respectively. All other reanalysis data sets are in close agreement with each other, with differences from the observations of between 0.5 and 1 K. The altitude and pressure of the cold point tropopause are captured best by ERA5, CFSR, MERRA, MERRA-2, and JRA-55, which all produce cold point tropopause levels that are slightly too low ($\sim$ 0.1 km). ERA-Interim, despite very good agreement in cold point temperature, shows slightly larger biases in cold point altitude ($\sim$ 0.2 km) relative to the GNSS-RO benchmark. Zonal mean cold point tropopause temperatures, altitudes, and pressures during 1981–1990 and 1991–2002 are shown for all reanalyses in Fig. S1 in the Supplement.

We investigate the temperature biases and their maxima near the Equator by analyzing latitude–longitude variations in the cold point tropopause relative to GNSS-RO estimates for four of the reanalyses (Fig. 7). To show differences at relatively high spatial resolution, we focus on the period 2007–2010. A wealth of observational studies has shown that the coldest tropopause temperatures are located over the "Maritime Continent" (i.e., the general area of Indonesia) and the western Pacific (Highwood and Hoskins, 1998), with secondary minima over equatorial South America and Africa coinciding with other centers of deep convective activity (Gettelman et al., 2002). The colocation of tropospheric convective activity with zonal asymmetries in cold point temperature can be explained by the radiative cooling effects of cirrus clouds overlying deep convection (Hartmann et al., 2001) or diabatic cooling associated with convective detrainment (Sherwood et al., 2003). Furthermore, it has been suggested that the response of equatorial waves to convective heating influences the structure of the cold point tropopause (Kim and Son, 2012; Nishimoto and Shiotani, 2012, 2013). The dominant wave modes responsible for cold point temperature variability are linked to equatorial Kelvin waves and the Madden–Julian Oscillation.

For the analyzed reanalyses (ERA5, ERA-Interim, MERRA-2, JRA–55, and CFSR), differences with respect to the observations are largest in the inner tropics over central Africa, reaching values of 50 % to 100 % greater than the zonal mean differences. This region is characterized by a local cold point minimum that results from deep convection and its interaction with equatorial waves. There is also evidence of a secondary maximum in the differences over equatorial South America or the eastern Pacific, although the

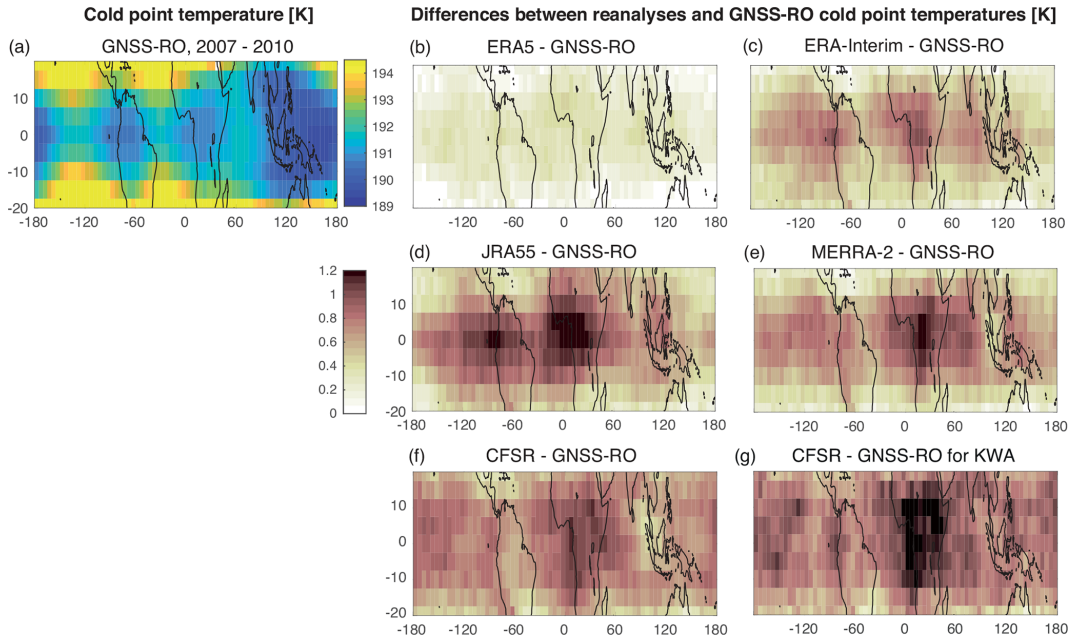

Figure 7. Latitude–longitude distributions during 2007–2010 of annual mean GNSS-RO cold point temperatures **(a)** and differences between cold point temperatures from individual reanalyses and those from GNSS-RO **(b–f)**. Differences between CFSR and GNSS-RO cold point temperatures for time periods of high Kelvin wave activity **(g)**.

magnitude and location of this maximum differ among the reanalyses.

The convective center over the western Pacific warm pool, where the cold point tropopause is coldest, does not show enhanced biases relative to the observations. One possible explanation for the bias distribution might link the enhanced temperature differences to Kelvin wave activity that maximizes over central Africa but is weaker over the western Pacific (Kim et al., 2019). As the Kelvin waves disturb the temperature profile at small vertical scales, the reanalyses may be particularly unsuited to estimate cold point temperatures in regions of strong Kelvin wave activity. We average cold point temperatures from reanalyses and observations over time periods of enhanced Kelvin wave activity. For CFSR, composite differences for periods with enhanced wave activity are compared in Fig. 7 to mean differences averaged over the whole 2007–2010 period. While mean biases over central Africa are less than 1 K, average differences during periods of enhanced Kelvin wave activity are as large as 1.4 K. The same is true for other reanalyses (not shown here), with the exception of ERA-Interim, suggesting that in most cases Kelvin waves contribute to the spatial structure of biases in cold point tropopause estimates based on reanalysis products.

The zonal mean lapse rate tropopause (Fig. 8) at the Equator is found at similar temperatures and heights as the cold point tropopause, being only slightly warmer and lower. Poleward of 10° S–10° N, however, the lapse rate tropopause height decreases considerably faster than the cold point height, since the cold point is more often located at the top of the inversion layer while the lapse rate tropopause is located at the bottom of the inversion layer (Seidel et al., 2001). Lapse rate tropopause temperatures based on reanalysis data are on average about 0.2 to 1.5 K too warm when compared to radio occultation data (see Fig. 3 and associated discussion) with best agreement for ERA5 and ERA-Interim. Consistent with this temperature bias, lapse rate tropopause levels based on reanalysis data are about 0.2 to 0.4 km lower than those based on radio occultation data. The latitudinal structure of lapse rate tropopause temperatures reveals slightly larger biases at the Equator and better agreement between 10 and 20° in each hemisphere and is generally very similar to the latitudinal distribution of biases in cold point temperatures (Fig. 6). The altitude of the lapse rate tropopause shows considerable meridional variability, ranging from 14.5 to 16.7 km. All reanalyses capture the plateau in lapse rate tropopause altitudes between 20° S and 20° N and the steep gradients in these altitudes on the poleward edges of the tropics. Zonal mean lapse rate tropopause temperatures, altitudes, and pressures during 1981–1990 and 1991–2002 are shown for all reanalyses in the Supplement Fig. S2.

4 Interannual variability and long-term changes

It has long been recognized that interannual variations in TTL temperatures are strongly affected by both tropospheric (e.g., ENSO) and stratospheric (e.g., QBO, solar, volcanic) variability (Randel et al., 2000; Zhou et al., 2001; Krüger

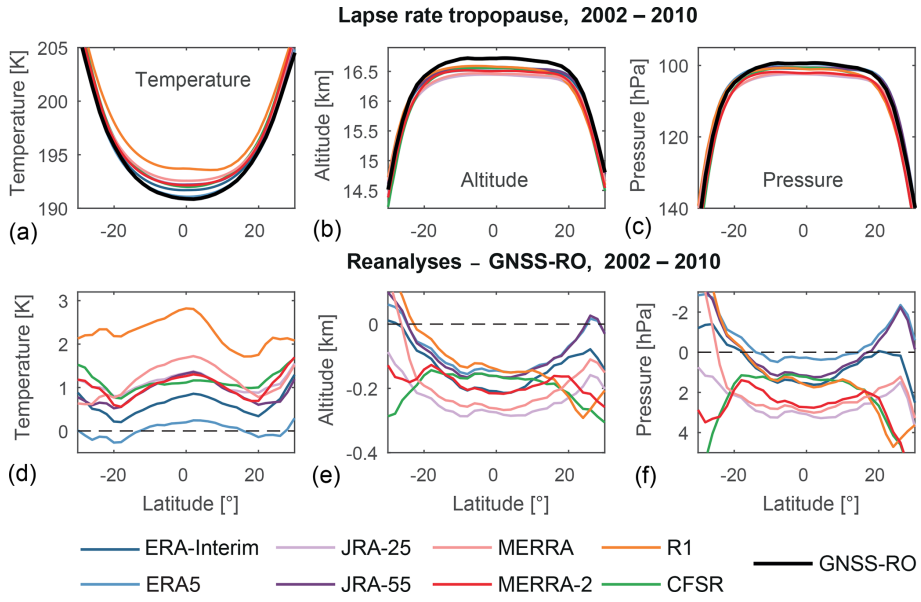

Figure 8. Latitudinal distributions of zonal-mean lapse rate tropopause temperature **(a)**, altitude **(b)**, and pressure **(c)** based on radio occultation data and reanalysis products during 2002–2010 **(a–c)**. Differences between radio occultation and reanalysis estimates are shown in the panels **(d)–(f)**.

et al., 2008). Time series of deseasonalized monthly 70 hPa temperature anomalies and cold point temperature, pressure, and altitude anomalies are shown in Fig. 9. Anomalies are calculated relative to the mean annual cycle during 2002–2010 for each data set. The interannual variability of ERA5 is not analyzed due to the short data record available at the time of the analysis. The performance of the reanalyses with respect to both the spread among reanalyses and their agreement with observations is much better at the 70 hPa level than at the cold point level. The older reanalyses NCEP-NCAR R1 and JRA-25 generally show larger deviations from the RAOBCORE time series. The level of agreement among the reanalyses and between reanalyses and observations improves over time, with a step-like improvement around 1998–1999 that is likely associated with the TOVS-to-ATOVS transition. The higher vertical resolution of measurements from the ATOVS suite (see Fig. 7 in Fujiwara et al., 2017) is known to reduce differences among the reanalysis with respect to stratospheric temperature (Long et al., 2017) and polar diagnostics (Lawrence et al., 2018). Within the TTL, temperature biases decrease from values of 1–2 K to around 0.5 K following the TOVS-to-ATOVS transition. This agreement improves further after 2002, when many of the more recent reanalyses started assimilating AIRS and GNSS-RO data (Table 1; see also Fig. 8 in Fujiwara et al., 2017).

Interannual variability at 70 hPa is dominated by the stratospheric QBO signal, which is reproduced by all reanalysis data sets. The amplitudes of the QBO temperature variations in all data sets based on multilinear regression analyses over 1981–2010 are shown in Fig. 10. At 70 hPa, the observational radiosonde data sets give QBO variations of 2.1–2.2 K. Reanalyses agree well with the observations and show QBO variations of 2–2.4 K. The only exception is NCEP-NCAR R1, which clearly underestimates the signal compared to radiosondes and other reanalyses, with an amplitude of 1.7 K. Best agreement with the radiosonde data sets is found for MERRA-2, MERRA, and CFSR. The influence of ENSO on TTL temperatures (not shown here) shows large longitudinal variations with positive anomalies over the Maritime Continent and western Pacific and negative anomalies over the eastern Pacific. While the zonally resolved response patterns agree well between observations and reanalyses, the zonal mean responses are not significant. Positive temperature anomalies following the eruptions of El Chichón in 1982 can be detected in Fig. 9 for all reanalyses, consistent with the results of Fujiwara et al. (2015). Following the Mount Pinatubo eruption in 1991, small positive temperature anomalies are evident at the 70 hPa level around the beginning of 1992. However, no positive temperature anomalies are found at the cold point during this time (see Fujiwara et al., 2015, for a more detailed analysis).

At the cold point, NCEP-NCAR R1 is a clear outlier, with much warmer temperature anomalies than any other data set during the period prior to 2005 (Fig. 9). However, differences among the more recent reanalyses are also relatively large, with ERA-Interim (on the lower side) and CFSR (on the upper side) showing differences as large as 2 K in the early years of the comparison. Given that existing homogenized radiosonde data sets also show deviations of up to 1.5 K at this level (Fig. 2 in Wang et al., 2012), we cannot deduce which reanalysis data set is most realistic. Note that the radiosonde time series from IGRA shown here should

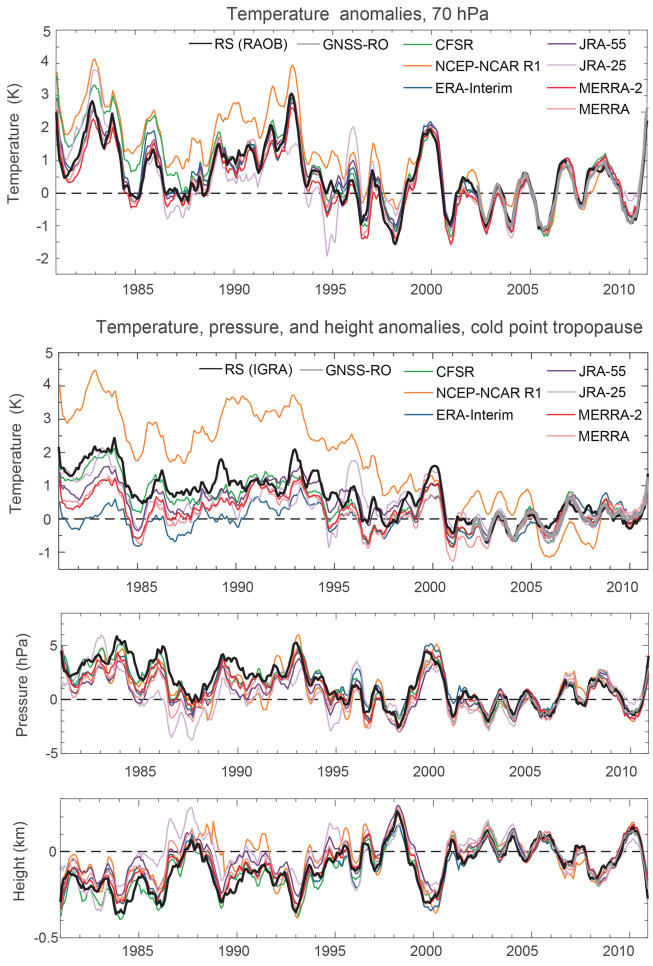

Figure 9. Time series of deseasonalized anomalies in 70 hPa temperature (upper), cold point temperature (upper middle), cold point pressure (lower middle), and cold point altitude (lower) averaged over the tropics (20° S–20° N) and evaluated relative to the reference period 2002–2010. Time series are shown for reanalysis products, radiosonde data (RAOBCORE and IGRA), and radio occultation data (GNSS-RO). Time series are smoothed with a 7-month running mean.

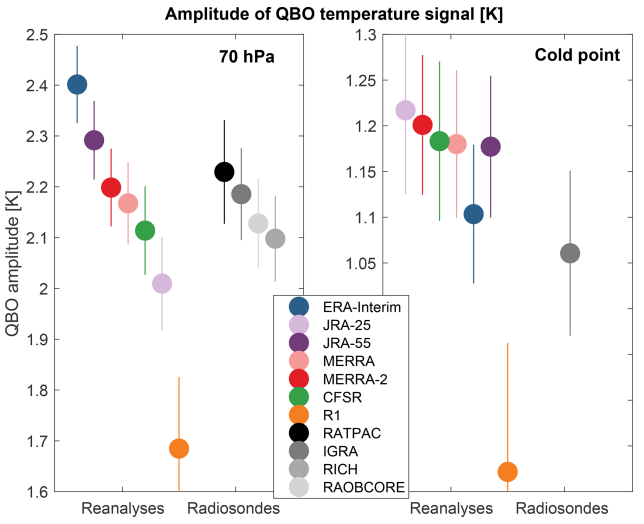

Figure 10. Amplitude of QBO temperature signal for 10° S–10° N at 70 hPa and the cold point derived from a multilinear regression analyses for radiosonde and reanalysis data sets for the period 1981–2010.

not be used for evaluating long-term changes (see Wang et al., 2012 for details) but only for assessing the representation of interannual variability. Periods of particularly pronounced interannual variability alternate with relatively quiescent ones. The amplitude of interannual variability (Fig. 9) and the QBO temperature signal (Fig. 10) are weaker at the cold point than at 70 hPa but are still well captured by all of the reanalysis data sets except for NCEP-NCAR R1.

Interannual variability in cold point pressure and altitude (Fig. 9) shows better agreement among the data sets than that in cold point or 70 hPa temperature. During the first 15 years of the record, the reanalysis cold point tropopause levels are mostly shifted toward lower altitudes and higher pressures, consistent with higher temperatures during this period. Anomalies in cold point temperature are in most cases matched by anomalies in cold point pressure and altitude, with a warmer cold point temperature (e.g., around 1999–2000) corresponding to lower tropopause (negative altitude anomaly and positive pressure anomaly) and vice versa. The older reanalyses NCEP-NCAR R1 and JRA-25 again show the largest overall differences. The agreement improves over time, with the most consistent results found for the period after 2002.

Long-term temperature changes are evaluated over the 1979–2005 time period due to the availability of adjusted tropopause trends from radiosonde data sets (see Wang et al., 2012 for details). Both radiosonde records suggest significant cooling at the 70 hPa level (Fig. 11). Trends derived from reanalysis data can be problematic due to changes in the assimilated observations. Given this potential limitation, it is of interest to examine whether the reanalysis trends are consistent with the hypothetically more reliable trends derived from homogenized observational records. At 70 hPa, temperature trends based on the reanalysis data sets span almost exactly the same range (−0.5 to −1.1 K per decade) as those based on the radiosonde data sets (−0.5 to −1 K per decade). All reanalysis-based and observationally based trends are significant at this level, confirming the stratospheric cooling reported by many previous studies (e.g., Randel et al., 2009). Satellite data from the microwave sounding unit (MSU) channel 4 (∼ 13–22 km) suggests smaller trends of around −0.25 K per decade over 1979–2005 (Maycock et al., 2018) or −0.4 K per decade over 1979–2009 (Emanuel et al., 2013). However, the much broader altitude range of this MSU channel includes both stratospheric and tropospheric levels, which impedes a direct comparison with trends at 70 hPa.

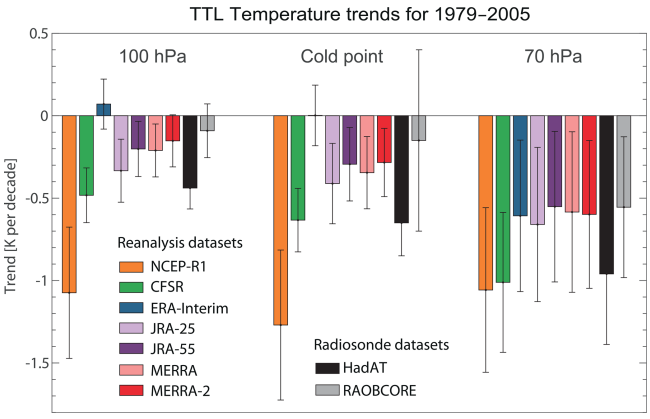

Figure 11. Linear trends in tropical mean (20° S–20° N) temperature (K per decade) at 100 hPa, the cold point, and 70 hPa for the time period 1979–2005. Error bars indicate $\pm 2\sigma$ uncertainty in the trend and account for serial autocorrelation.

At the cold point, the situation is completely different. The available adjusted radiosonde data sets show in some cases uncertainties larger than the respective temperature trends at these levels. Only a few of the available data sets indicate a statistically significant cooling based on a methodology that adjusts the cold point trend to account for nearby fixed pressure-level data and day–night differences (Wang et al., 2012). Based on the trends shown in Wang et al. (2012) for five adjusted radiosonde data sets, we show here the smallest and largest reported trends and consider their range (including the reported error bars) as the observational uncertainty range. Similar to the observations, the reanalysis data sets suggest a large range in cold point temperature trends, from no trend at all (0 K per decade for ERA-Interim) to a strong cooling of −1.3 K per decade (NCEP-NCAR R1). The latter is outside of the observational uncertainty range and can thus be considered unrealistic. All other reanalyses suggest small but significant cooling trends of −0.3 to −0.6 K per decade. JRA-25, JRA-55, MERRA, and MERRA-2 agree particularly well and produce trends in the middle of the observational uncertainty range. Overall, due to the large uncertainties in radiosonde-derived cold point temperature trends, all reanalyses except for R1 are statistically consistent with at least one of the observational data sets.

Temperature trends at 100 hPa are very similar to trends at the cold point level, and again they suggest consistency among most of the reanalysis and radiosonde data sets, with the notable exception of R1. Nearly all data sets suggest slightly smaller cooling trends (−0.15 to −0.5 K per decade) relative to the cold point consistent with the fact that the cold point is at slightly higher altitudes than 100 hPa. Among the data sets, only ERA-Interim produces a warming trend (0.07 K per decade), although this result is not statistically significant.

5 Summary

Meteorological reanalyses are widely used in scientific studies of TTL processes being utilized as "stand in observations" or for driving transport models. The most recent atmospheric reanalysis data sets (ERA5, ERA-Interim, MERRA-2, JRA-55, and CFSR) all provide realistic representations of the major characteristics of temperature structure within the TTL for 2002–2010. There is good agreement between reanalysis estimates of tropical mean temperatures between 140 and 70 hPa and GNSS-RO retrievals, with relatively small cold biases for most data sets. CFSR shows the best agreement with GNSS-RO in this layer with a mean bias of −0.06 K. Agreement between the temperature profiles and the GNSS-RO data clearly improves when the comparison is restricted to the period after 2007, when the densely sampled COSMIC data were assimilated by all reanalyses.

Temperatures at the cold point and lapse rate tropopause levels show warm biases in reanalyses when compared to observations. This tropopause-level warm bias is opposite to the cold bias found at all model levels and is most likely related to difficulties in determining the true cold point and lapse rate tropopause levels from discrete temperature profiles with coarse vertical resolution. Our analysis confirms that the magnitude of the bias shift is consistent with the vertical resolution of the reanalysis data, with the smallest bias shifts found for data sets with the highest vertical resolution around the tropopause (ERA5 and CFSR). The negative temperature bias at model levels is often canceled out by the positive bias introduced when identifying the lapse rate and cold point tropopause locations. As a result, ERA5, which has a small negative bias at model levels and a small bias shift, has the most realistic tropopause temperatures, while CFSR, which produces the most realistic model-level temperature profile, has a warm bias of 0.6–0.9 K at the cold point and lapse rate tropopause levels. Older reanalyses like MERRA, JRA-25, and especially NCEP-NCAR R1 show the largest temperature biases at the tropopause levels.

The zonal structure of tropopause temperature reveals that the biases in reanalysis relative to observations maximize at or near the Equator. All of the recent reanalyses produce a realistic horizontal structure of cold point temperature with minima corresponding to the centers of tropical deep convection. Differences between reanalyses and observations are greatest over equatorial Africa. These enhanced differences are possibly related to Kelvin wave activity and associated disturbances in TTL temperatures that also maximize in this region. Further investigation of seasonal variability in the cold point tropopause, including detailed analysis of this feature, will be conducted in a follow-up study.

Interannual variability in reanalysis temperatures is best constrained in the upper TTL (70 hPa), with larger differences at lower levels such as the cold point and 100 hPa. The reanalyses reproduce the temperature responses to major dynamical and radiative signals such as volcanic eruptions and

the QBO. Agreement among the reanalyses and between the reanalyses and observations generally improves over time, with a step-like improvement around the TOVS-to-ATOVS transition in 1998–1999 and in 2006 with the beginning of the assimilation of COSMIC GNSS-RO data. Interannual variability is lower at the cold point and 100 hPa relative to 70 hPa but with larger month-to-month fluctuations causing larger discrepancies among the reanalyses. As at 70 hPa, NCEP-NCAR R1 is a clear outlier. Interannual variability in cold point pressure and altitude shows better agreement than that in TTL temperature. Anomalies in cold point temperatures are in most cases matched by corresponding anomalies in cold point pressure and altitude.

Long-term reanalysis trends in temperature at 70 hPa show good agreement with trends derived from adjusted radiosonde data sets. All reanalyses and observational data sets indicate significant stratospheric cooling at this level of around -0.5 to -1 K per decade. At the 100 hPa and cold point levels, both adjusted radiosonde data sets and reanalyses indicate large uncertainties in temperature trends. Reanalysis-based estimates at the cold point range from no trend at all (0 K per decade for ERA-Interim) to strong cooling of -1.3 K per decade (NCEP-NCAR R1). While the latter is outside of the observational uncertainty range and can be considered unrealistic, all other reanalysis data sets agree with at least one of the observational data sets within uncertainties. The bulk of the reanalyses are in good agreement at these levels, suggesting small but significant cooling trends of -0.3 to -0.6 K per decade that are statistically consistent with trends based on the adjusted radiosonde data sets.

Advances of the reanalysis and observational systems over the last decades have led to a clear improvement in the TTL reanalyses products over time. In particular, the more recent reanalyses (ERA-Interim, ERA5, MERRA-2, CFSR, and JRA-55) mostly show very good agreement after 2002 in terms of the vertical TTL temperature profile, meridional tropopause structure, and interannual variability. Temperatures at the cold point and lapse rate, on the other hand, are too high for most reanalyses, regardless of production date. As these differences maximize over central Africa, a center of deep convective activity, chemical transport models driven by reanalyses and simulating air mass transport into the stratosphere can be expected to have too little dehydration and too high water vapor. Furthermore, all reanalyses place the cold point tropopause too low in altitude relative to observations. This displacement can have important implications for studies that compare water vapor and ice observations with the position of the cold point tropopause derived from reanalyses data, as enhanced ice and water vapor contents could be erroneously attributed to deep convection crossing the tropopause.

Depending on the particular application, different reanalyses offer different advantages such as a realistic cold point temperature (e.g., ERA5), small bias in the TTL temperature profile (e.g., CFSR), realistic spatial distribution of the cold point temperature (e.g., ERA-Interim), continuous TTL temperature time series through 2006 (e.g., JRA55), or a realistic representation of signals of interannual variability (e.g., MERRA-2). Their use in model simulations and in comparisons with climate model output should be tailored to their specific strengths and weaknesses.

Data availability. Reanalyses, GNSS-RO, and radiosonde data can be inquired about by contacting the authors.

Supplement. The supplement related to this article is available online at: https://doi.org/10.5194/acp-20-753-2020-supplement.

Author contributions. ST developed the idea for this paper and carried out the evaluations with contributions from all co-authors. SD and BL provided the reanalyses tropopause and profile data. RPK provided the GNSS-RO tropopause, wave activity, and temperature profile data. JaSW provided the radiosonde tropopause data. ST wrote the article with contributions from all co-authors.

Competing interests. The authors declare that they have no conflict of interest.

Special issue statement. This article is part of the special issue "The SPARC Reanalysis Intercomparison Project (S-RIP) (ACP/ESSD inter-journal SI)". It is not associated with a conference.

Acknowledgements. We thank the reanalysis centers for providing their support and data products. We thank Christine Bloecker from the Global Modeling and Assimilation Office, NASA Goddard Space Flight Center for providing information on the GNSS-RO data assimilated in MERRA-2. ERA5 data were generated using Copernicus Climate Change Service Information. MERRA-2 data access was through the Global Modeling and Assimilation Office (GMAO, 2015). The work of Susann Tegtmeier was funded by the Deutsche Forschungsgemeinschaft (DFG, German Research Foundation) – TE 1134/1. Contributions from James S. Wright were supported by the National Natural Science Foundation of China (20171352419) via a joint DFG–NSFC funding initiative.

Financial support. The article processing charges for this open-access publication were partially covered by University of Saskatchewan funding.

The article processing charges for this open-access publication were covered by a Research Centre of the Helmholtz Association.

Review statement. This paper was edited by Peter Haynes and reviewed by four anonymous referees.

References

Anthes, R. A., Bernhardt, P. A., Chen, Y., Cucurull, L., Dymond, K. F., Ector, D., Healy, S. B., Ho, S.-P., Hunt, D. C., Kuo, Y.-H., Liu, H., Manning, K., McCormick, C., Meehan, T. K., Randel, W. J., Rocken, C., Schreiner, W. S., Sokolovskiy, S. V., Syndergaard, S., Thompson, D. C., Trenberth, K. E., Wee, T.-K., Yen, N. L., and Zeng, Z.: The COSMIC/FORMOSAT-3 Mission: Early Results, B. Am. Meteor. Soc., 89, 313–333, https://doi.org/10.1175/BAMS-89-3-313, 2008.

Beyerle, G., Schmidt, T., Michalak, G., Heise, S., Wickert, J., and Reigber, C.: GPS radio occultation with GRACE: Atmospheric profiling utilizing the zero difference technique, Geophys. Res. Lett., 32, L13806, https://doi.org/10.1029/2005GL023109, 2005.

Beyerle, G., Grunwaldt, L., Heise, S., Köhler, W., König, R., Michalak, G., Rothacher, M., Schmidt, T., Wickert, J., Tapley, B. D., and Giesinger, B.: First results from the GPS atmosphere sounding experiment TOR aboard the TerraSAR-X satellite, Atmos. Chem. Phys., 11, 6687–6699, https://doi.org/10.5194/acp-11-6687-2011, 2011.

Chipperfield, M. P.: Multiannual simulations with a three-dimensional chemical transport model, J. Geophys. Res., 104, 1781–1805, https://doi.org/10.1029/98JD02597, 1999.

Cucurull, L., Derber, J. C., and Purser, R. J.: A bending angle forward operator for global positioning system radio occultation measurements, J. Geophys. Res.-Atmos., 118, 14–28, https://doi.org/10.1029/2012JD017782, 2013.

Dee, D. P., Uppala, S. M., Simmons, A. J., Berrisford, P., Poli, P., Kobayashi, S., Andrae, U., Balmaseda, M. A., Balsamo, G., Bauer, P., Bechtold, P., Beljaars, A. C. M., van de Berg, L., Bidlot, J., Bormann, N., Delsol, C., Dragani, R., Fuentes, M., Geer, A. J., Haimberger, L., Healy, S. B., Hersbach, H., Hólm, E. V., Isaksen, L., Kållberg, P., Köhler, M., Matricardi, M., McNally, A. P., Monge-Sanz, B. M., Morcrette, J.-J., Park, B.-K., Peubey, C., de Rosnay, P., Tavolato, C., Thépaut, J.-N., and Vitart, F.: The ERA-Interim reanalysis: configuration and performance of the data assimilation system, Q. J. Roy. Meteorol. Soc., 137, 553–597, https://doi.org/10.1002/qj.828, 2011.

Durre, I., Vose, R. S., and Wuertz, D. B.: Overview of the Integrated Global Radiosonde Archive, J. Climate, 19, 53–68, https://doi.org/10.1175/JCLI3594.1, 2006.

Efron, B. and Tibshirani, R. J.: An Introduction to the Bootstrap, Chapman and Hall, New York, 436 pp., 1993.

Emanuel, K., Solomon, S., Folini, D., Davis, S., and Cagnazzo, C.: Influence of Tropical Tropopause Layer Cooling on Atlantic Hurricane Activity, J. Climate, 26, 2288–2301, https://doi.org/10.1175/JCLI-D-12-00242.1, 2013.

Folkins, I., Lowewenstein, M., Podolske, J., Oltmans, S., and Proffitt, M.: A barrier to vertical mixing at 14 km in the tropics: Evidence from ozonesondes and aircraft measurements, J. Geophys. Res., 104, 22095–22102, 1999.

Free, M., Seidel, D. J., Angell, J. K., Lanzante, J., Durre, I., and Peterson, T. C.: Radiosonde Atmospheric Temperature Products for Assessing Climate (RATPAC): A new data set of large-area anomaly time series, J. Geophys. Res., 110, D22101, https://doi.org/10.1029/2005JD006169, 2005.

Fueglistaler, S., Dessler, A., Dunkerton, T., Folkins, I., Fu, Q., and Mote, P. W.: Tropical tropopause layer, Rev. Geophys., 47, 1004, https://doi.org/10.1029/2008RG000267, 2009.

Fueglistaler, S., Haynes, P. H., and Forster, P. M.: The annual cycle in lower stratospheric temperatures revisited, Atmos. Chem. Phys., 11, 3701–3711, https://doi.org/10.5194/acp-11-3701-2011, 2011.

Fujiwara, M., Suzuki, J., Gettelman, A., Hegglin, M. I., Akiyoshi, H., and Shibata, K.: Wave activity in the tropical tropopause layer in seven reanalysis and four chemistry climate model data sets, J. Geophys. Res., 117, D12105, https://doi.org/10.1029/2011JD016808, 2012.

Fujiwara, M., Hibino, T., Mehta, S. K., Gray, L., Mitchell, D., and Anstey, J.: Global temperature response to the major volcanic eruptions in multiple reanalysis data sets, Atmos. Chem. Phys., 15, 13507–13518, https://doi.org/10.5194/acp-15-13507-2015, 2015.

Fujiwara, M., Wright, J. S., Manney, G. L., Gray, L. J., Anstey, J., Birner, T., Davis, S., Gerber, E. P., Harvey, V. L., Hegglin, M. I., Homeyer, C. R., Knox, J. A., Krüger, K., Lambert, A., Long, C. S., Martineau, P., Molod, A., Monge-Sanz, B. M., Santee, M. L., Tegtmeier, S., Chabrillat, S., Tan, D. G. H., Jackson, D. R., Polavarapu, S., Compo, G. P., Dragani, R., Ebisuzaki, W., Harada, Y., Kobayashi, C., McCarty, W., Onogi, K., Pawson, S., Simmons, A., Wargan, K., Whitaker, J. S., and Zou, C.-Z.: Introduction to the SPARC Reanalysis Intercomparison Project (S-RIP) and overview of the reanalysis systems, Atmos. Chem. Phys., 17, 1417–1452, https://doi.org/10.5194/acp-17-1417-2017, 2017.

Gelaro, R., McCarty, W., Suárez, M. J., Todling, R., Molod, A., Takacs, L., Randles, C. A., Darmenov, A., Bosilovich, M. G., Reichle, R., Wargan, K., Coy, L., Cullather, R., Draper, C., Akella, S., Buchard, V., Conaty, A.,da Silva, A. M., Gu, W., Kim, G., Koster, R., Lucchesi, R., Merkova, D., Nielsen, J. E., Partyka, G., Pawson. S., Putman, W., Rienecker, M., Schubert, S. D., Sienkiewicz, M., and Zhao, B.: The Modern-Era Retrospective Analysis for Research and Applications, Version 2 (MERRA-2), J. Climate, 30, 5419–5454, https://doi.org/10.1175/JCLI-D-16-0758.1, 2017.

Gettelman, A., Salby, M. L., and Sassi, F.: Distribution and influence of convection in the tropical tropopause region, J. Geophys. Res., 107, 4080, https://doi.org/10.1029/2001JD001048, 2002.

Gettelman, A., Hegglin, M. I., Son, S.-W., Kim, J., Fujiwara, M., Birner, T., Kremser, S., Rex, M., Añel, J. A., Akiyoshi, H., Austin, J., Bekki, S., Braesike, P., Brühl, C., Butchart, N., Chipperfield, M., Dameris, M., Dhomse, S., Garny, H., Hardiman, S. C., Jöckel, P., Kinnison, D. E., Lamarque, J. F., Mancini, E., Marchand, M., Michou, M., Morgenstern, O., Pawson, S., Pitari, G., Plummer, D., Pyle, J. A., Rozanov, E., Scinocca, J., Shepherd, T. G., Shibata, K., Smale, D., Teyssèdre, H., and Tian, W.: Multimodel assessment of the upper troposphere and lower stratosphere: Tropics and global trends, J. Geophys. Res., 115, D00M08, https://doi.org/10.1029/2009JD013638, 2010.

Global Modeling and Assimilation Office (GMAO), MERRA-2 inst6_3d_ana_Nv: 3d, 6-Hourly, Instantaneous, Model-Level, Analysis, Analyzed Meteorological Fields V5.12.4, Greenbelt, MD, USA, Goddard Earth Sciences Data and Infor-

mation Services Center (GES DISC), Accessed: [1.1.2015], https://doi.org/10.5067/IUUF4WB9FT4W, 2015.

Gorbunov, M. E., Benzon, H.-H., Jensen, A. S., Lohmann, M. S., and Nielsen, A. S.: Comparative analysis of radio occultation processing approaches based on Fourier integral operators, Radio Sci., 39, RS6004, https://doi.org/10.1029/2003RS002916, 2004.

Haimberger, L.: Homogenization of Radiosonde Temperature Time Series Using Innovation Statistics, J. Climate, 20, 1377–1403, https://doi.org/10.1175/JCLI4050.1, 2007.

Haimberger, L., Tavolato, C., and Sperka, S.: Homogenization of the Global Radiosonde Temperature Dataset through Combined Comparison with Reanalysis Background Series and Neighboring Stations, J. Climate, 25, 8108–3131, https://doi.org/10.1175/JCLI-D-11-00668.1, 2012.

Hajj, G. A., Ao, C. O., Iijima, B. A., Kuang, D., Kursinski, E. R., Mannucci, A. J., Meehan, T. K., Romans, L. J., de la Torre Juarez, M., and Yunck, T. P.: CHAMP and SAC-C atmospheric occultation results and intercomparisons, J. Geophys. Res.-Atmos., 109, D06109, https://doi.org/10.1029/2003JD003909, 2004.

Hartmann, D. L., Holton, J. R., and Fu, Q.: The heat balance of the tropical tropopause, cirrus, and stratospheric dehydration, Geophys. Res. Lett., 28, 1969–1972, 2001.

Hersbach, H., de Rosnay, P., Bell, B., Schepers, D., Simmons, A., Soci, C., Abdalla, S., Alonso-Balmaseda, M., Balsamo, G., Bechtold, P., Berrisford, P., Bidlot, J.-R., de Boisséson, E., Bonavita, M., Browne, P., Buizza, R., Dahlgren, P., Dee, D., Dragani, R., Diamantakis, M., Flemming, J., Forbes, R., Geer, A. J., Haiden, T., Hólm, E., Haimberger, L., Hogan, R., Horányi, A., Janiskova, M., Laloyaux, P., Lopez, P., Munoz-Sabater, J., Peubey, C., Radu, R., Richardson, D., Thépaut, J.-N., Vitart, F., Yang, X., Zsótér, E., and Zuo, H.: Operational global reanalysis: progress, future directions and synergies with NWP, ERA Report Series, 27, 2018.

Highwood, E. J. and Hoskins, B. J.: The tropical tropopause, Q. J. Roy. Meteorol. Soc., 124, 1579–1604, https://doi.org/10.1002/qj.49712454911, 1998.

Ho, S.-P., Peng, L., and Vömel, H.: Characterization of the long-term radiosonde temperature biases in the upper troposphere and lower stratosphere using COSMIC and Metop-A/GRAS data from 2006 to 2014, Atmos. Chem. Phys., 17, 4493–4511, https://doi.org/10.5194/acp-17-4493-2017, 2017.

Holton, J. R. and Gettelman, A.: Horizontal transport and the dehydration of the stratosphere, Geophys. Res. Lett., 28, 2799–2802, 2001.

Kim, J. and Son, S.: Tropical Cold-Point Tropopause: Climatology, Seasonal Cycle, and Intraseasonal Variability Derived from COSMIC GPS Radio Occultation Measurements, J. Climate, 25, 5343–5360, https://doi.org/10.1175/JCLI-D-11-00554.1, 2012.

Kim, Y.-H., Kiladis, G. N., Albers, J. R., Dias, J., Fujiwara, M., Anstey, J. A., Song, I.-S., Wright, C. J., Kawatani, Y., Lott, F., and Yoo, C.: Comparison of equatorial wave activity in the tropical tropopause layer and stratosphere represented in reanalyses, Atmos. Chem. Phys., 19, 10027–10050, https://doi.org/10.5194/acp-19-10027-2019, 2019.

Kistler, R., Collins, W., Saha, S., White, G., Woollen, J., Kalnay, E., Chelliah, M., Ebisuzaki, W., Kanamitsu, M., Kousky, V., van den Dool, H., Jenne, R., and Fiorino, M.: The NCEP–NCAR 50-year reanalysis: monthly means CD-ROM and documentation, B. Am. Meteor. Soc., 82, 247–267, 2001.

Kobayashi, S., Ota, Y., Harada, Y., Ebita, A., Moriya, M., Onoda, H., Onogi, K., Kamahori, H., Kobayashi, C., Endo, H., Miyaoka, K., and Takahashi, K.: The JRA-55 reanalysis: general specifications and basic characteristics, J. Meteorol. Soc. Jpn., 93, 5–48, https://doi.org/10.2151/jmsj.2015-001, 2015.

Krüger, K., Tegtmeier, S., and Rex, M.: Long-term climatology of air mass transport through the Tropical Tropopause Layer (TTL) during NH winter, Atmos. Chem. Phys., 8, 813–823, https://doi.org/10.5194/acp-8-813-2008, 2008.

Krüger, K., Tegtmeier, S., and Rex, M.: Variability of residence time in the Tropical Tropopause Layer during Northern Hemisphere winter, Atmos. Chem. Phys., 9, 6717–6725, https://doi.org/10.5194/acp-9-6717-2009, 2009.

Kursinski, E. R., Hajj, G. A., Schofield, J. T., Linfield, R. P., and Hardy, K. R.: Observing Earth's atmosphere with radio occultation measurements using the Global Positioning System, J. Geophys. Res.-Atmos., 102, 23429–23465, https://doi.org/10.1029/97JD01569, 1997.

Lawrence, Z. D., Manney, G. L., and Wargan, K.: Reanalysis intercomparisons of stratospheric polar processing diagnostics, Atmos. Chem. Phys., 18, 13547–13579, https://doi.org/10.5194/acp-18-13547-2018, 2018.

Long, C. S., Fujiwara, M., Davis, S., Mitchell, D. M., and Wright, C. J.: Climatology and interannual variability of dynamic variables in multiple reanalyses evaluated by the SPARC Reanalysis Intercomparison Project (S-RIP), Atmos. Chem. Phys., 17, 14593–14629, https://doi.org/10.5194/acp-17-14593-2017, 2017.

Maycock, A. C., Randel, W. J., Steiner, A. K., Karpechko, A. Y., Cristy, J., Saunders, R., Thompson, D. W. J., Zou, C.-Z., Chrysanthou, A., Abraham, N. L., Akiyoshi, H., Archibald, A. T., Butchart, N., Chipperfield, M., Dameris, M., Deushi, M., Dhomse, S., Di Genova, G., Jo¨ckel, P., Kinnison, D. E., Kirner, O., Ladsta¨dter, F., Michou, M., Morgenstern, O., O'Connor, F., Oman, L., Pitari, G., Plummer, D. A., Revell, L. E., Rozanov, E., Stenke, A., Visioni, D., Yamashita, Y., and Zeng, G.: Revisiting the mystery of recent stratospheric temperature trends, Geophys. Res. Lett., 1–15, https://doi.org/10.1029/2018GL078035, 2018.

Mote, P. W., Rosenlof, K. H., McIntyre, M. E., Carr, E. S., Gille, J. C., Holton, J. R., Kinnersley, J. S., Pumphrey, H. C., Russell, J. M., and Waters, J. W.: An atmospheric tape recorder: The imprint of tropical tropopause temperatures on stratospheric water vapor, J. Geophys. Res., 101, 3989–4006, https://doi.org/10.1029/95JD03422, 1996.

Nash, J., Oakley, T., Vömel, H., and Li, W.: WMO intercomparison of high-quality radiosonde systems, Yangjiang, China, 12 July–3 August 2010, Instruments and Observing Methods Re- port No. 107, WMO/TD-No. 1580, WMO, Geneva, Switzerland, 238 pp., 2011.

Naujokat, B.: An update of the observed quasi-biennial oscillation of the stratospheric winds over the tropics, J. Atmos. Sci., 43, 1873–1877, 1986.

Nishimoto, E. and Shiotani, M.: Seasonal and interannual variability in the temperature structure around the tropical tropopause and its relationship with convective activities, J. Geophys. Res.-Atmos., 117, D02104, https://doi.org/10.1029/2011JD016936, 2012.

Nishimoto, E. and Shiotani, M.: Intraseasonal variations in the tropical tropopause temperature revealed by cluster analysis of

convective activity, J. Geophys. Res.-Atmos., 118, 3545–3556, https://doi.org/10.1002/jgrd.50281, 2013.

Onogi, K., Tsutsui, J., Koide, H., Sakamoto, M., Kobayashi, S., Hatsushika, H., Matsumoto, T., Yamazaki, N., Kamahori, H., Takahashi, K., Kadokura, S., Wada, K., Kato, K., Oyama, R., Ose, T., Mannoji, N., and Taira, R.: The JRA-25 reanalysis, J. Meteorol. Soc. Jpn., 85, 369–432, https://doi.org/10.2151/jmsj.85.369, 2007.

Pan, L. L. and Munchak, L. A.: Relationship of cloud top to the tropopause and jet structure from CALIPSO data, J. Geophys. Res., 116, D12201, https://doi.org/10.1029/2010JD015462, 2011.

Pan, L. L., Honomichl, S. B., Bui, T. V., Thornberry, T., Rollins, A., Hintsa, E., and Jensen, E. J.: Lapse Rate or Cold Point: The Tropical Tropopause Identified by In Situ Trace Gas Measurements, Geophys. Res. Lett., 45, 10756–10763, https://doi.org/10.1029/2018GL079573, 2018.

Randel W. J. and Jensen, E.: Physical processes in the tropical tropopause layer and their roles in a changing climate, Nat. Geosci., 6, 169–176, 2013.

Randel, W. J., Wu, F., and Gaffen, D. J.: Low frequency variations of the tropical tropopause from NCEP reanalyses, J. Geophys. Res., 105, 15509–15523, 2000.

Randel, W. J., Wu, F., Oltmans, S. J., Rosenlof, K., and Nedoluha, G. E.: Interannual Changes of Stratospheric Water Vapor and Correlations with Tropical Tropopause Temperatures, J. Atmos. Sci., 61, 2133–2148, https://doi.org/10.1175/1520-0469(2004)061<2133:ICOSWV>2.0.CO;2, 2004a.

Randel, W. J., Udelhofen, P., Fleming, E., Geller, M., Gelman, M., Hamilton, K., Karoly, D., Ortland, D., Pawson, S., Swinbank, R., Wu, F., Baldwin, M., Chanin, M., Keckhut, P., Labitzke, K., Remsberg, E., Simmons, A., and Wu, D.: The SPARC Intercomparison of Middle-Atmosphere Climatologies, J. Climate, 17, 986–1003, https://doi.org/10.1175/1520-0442(2004)017<0986:TSIOMC>2.0.CO;2, 2004b.

Randel, W. J., Shine, K. P., Austin, J., Barnett, J., Claud, C., Gillett, N. P., Keckhut, P., Langematz, U., Lin, R., Long, C., Mears, C., Miller, A., Nash, J., Seidel, D. J., Thompson, D. W. J., Wu, F., and Yoden, S.: An update of observed stratospheric temperature trends, J. Geophys. Res., 114, D02107, https://doi.org/10.1029/2008JD010421, 2009.

Rienecker, M. M., Suarez, M. J., Gelaro, R., Todling, R., Bacmeister, J., Liu, E., Bosilovich, M. G., Schubert, S. D., Takacs, L., Kim, G.-K., Bloom, S., Chen, J., Collins, D., Conaty, A., da Silva, A., Gu, W., Joiner, J., Koster, R. D., Lucchesi, R., Molod, A., Owens, T., Pawson, S., Pegion, P., Redder, C. R., Reichle, R., Robertson, F. R., Ruddick, A. G., Sienkiewicz, M., and Woollen, J.: MERRA: NASA's modern-era retrospective analysis for research and applications, J. Climate, 24, 3624–3648, https://doi.org/10.1175/JCLI-D-11-00015.1, 2011.

Saha, S., Moorthi, S., Pan, H.-L., Wu, X., Wang, J., Nadiga, S., Tripp, P., Kistler, R., Woollen, J., Behringer, D., Liu, H., Stokes, D., Grumbine, R., Gayno, G., Wang, J., Hou, Y.-T., Chuang, H.-Y., Juang, H.-M. H., Sela, J., Iredell, M., Treadon, R., Kleist, D., van Delst, P., Keyser, D., Derber, J., Ek, M., Meng, J., Wei, H., Yang, R., Lord, S., van den Dool, H., Kumar, A., Wang, W., Long, C., Chelliah, M., Xue, Y., Huang, B., Schemm, J.-K., Ebisuzaki, W., Lin, R., Xie, P., Chen, M., Zhou, S., Higgins, W., Zou, C.-Z., Liu, Q., Chen, Y., Han, Y., Cucurull, L., Reynolds, R. W., Rutledge, G., and Goldberg, M.: The NCEP climate forecast system reanalysis, B. Am. Meteor. Soc., 91, 1015–1057, https://doi.org/10.1175/2010BAMS3001.1, 2010.

Santer, B. D., Sausen, R., Wigley, T. M. L., Boyle, J. S., AchutaRao, K., Doutriaux, C., Hansen, J. E., Meehl, G. A., Roeckner, E., Ruedy, R., Schmidt, G., and Taylor, K.E.: Behavior of tropopause height and atmospheric temperature in models, reanalyses, and observations: Decadal changes, J. Geophys. Res., 108, 4002, https://doi.org/10.1029/2002JD002258, 2003.

Schoeberl, M. R., Dessler, A. E., and Wang, T.: Simulation of stratospheric water vapor and trends using three reanalyses, Atmos. Chem. Phys., 12, 6475–6487, https://doi.org/10.5194/acp-12-6475-2012, 2012.

Seidel, D. J. and Randel, W. J.: Variability and trends in the global tropopause estimated from radiosonde data, J. Geophys. Res., 111, D21101, https://doi.org/10.1029/2006JD007363, 2006.

Seidel, D. J., Ross, R. J., Angell, J. K., and Reid, G. C.: Climatological characteristics of the tropical tropopause as revealed by radiosondes, J. Geophys. Res., 106, 7857–7878, https://doi.org/10.1029/2000JD900837, 2001.

Sherwood, S. C., Horinouchi, T., and Zeleznik, H. A.: Convective impact on temperatures observed near the tropical tropopause, J. Atmos. Sci., 60, 1847–1856, 2003.

Simmons, A. J., Poli, P., Dee, D. P., Berrisford, P., Hersbach, H., Kobayashi, S., and Peubey, C.: Estimating low-frequency variability and trends in atmospheric temperature using ERA-Interim, Q. J. Roy. Meteorol. Soc., 140, 329–353, https://doi.org/10.1002/qj.2317, 2014.

Tao, M., Konopka, P., Ploeger, F., Yan, X., Wright, J. S., Diallo, M., Fueglistaler, S., and Riese, M.: Multitimescale variations in modeled stratospheric water vapor derived from three modern reanalysis products, Atmos. Chem. Phys., 19, 6509–6534, https://doi.org/10.5194/acp-19-6509-2019, 2019.

Thorne, P. W., Parker, D. E., Tett, S. F. B., Jones, P. D., McCarthy, M., Coleman, H., and Brohan, P.: Revisiting radiosonde upper air temperatures from 1958 to 2002, J. Geophys. Res., 110, D18105, https://doi.org/10.1029/2004JD005753, 2005.

Thomason, L. W., Ernest, N., Millán, L., Rieger, L., Bourassa, A., Vernier, J.-P., Manney, G., Luo, B., Arfeuille, F., and Peter, T.: A global space-based stratospheric aerosol climatology: 1979–2016, Earth Syst. Sci. Data, 10, 469–492, https://doi.org/10.5194/essd-10-469-2018, 2018.

von Engeln, A., Andres, Y., Marquardt, C., and Sancho, F.: GRAS radio occultation on-board of Metop, Adv. Space Res., 47, 336–347, https://doi.org/10.1016/j.asr.2010.07.028, 2011.

Wang, J. S., Seidel, D. J., and Free, M., How well do we know recent climate trends at the tropical tropopause?, J. Geophys. Res., 117, D09118, https://doi.org/10.1029/2012JD017444, 2012.

Wheeler, M. and Kiladis, G.N.: Convectively Coupled Equatorial Waves: Analysis of Clouds and Temperature in the Wavenumber–Frequency Domain, J. Atmos. Sci., 56, 374–399, https://doi.org/10.1175/1520-0469(1999)056<0374:CCEWAO>2.0.CO;2, 1999.

Wickert, J., Reigber, C., Beyerle, G., König, R., Marquardt, C., Schmidt, T., Grunwaldt, L., Galas, R., Meehan, T. K., Melbourne, W. G., and Hocke, K.: Atmosphere sounding by GPS radio occultation: First results from CHAMP, Geophys. Res. Lett., 28, 3263–3266, https://doi.org/10.1029/2001GL013117, 2001.

World Meteorological Organization: Definition of the tropopause, Bulletin of the World Meteorological Organization, 6, 136–137, 1957.

Wright, C. J. and Hindley, N. P.: How well do stratospheric reanalyses reproduce high-resolution satellite temperature measurements?, Atmos. Chem. Phys., 18, 13703–13731, https://doi.org/10.5194/acp-18-13703-2018, 2018.

Xie, F., Li, J., Tian, W., Li, Y., and Feng, J.: Indo-Pacific warm pool area expansion, Modoki activity, and tropical cold-point tropopause temperature variations, Sci. Rep., 4, 4552, https://doi.org/10.1038/srep04552, 2014.

Zhou, X. L., Geller, M. A., and Zhang, M. H.: Tropical Cold Point Tropopause Characteristics Derived from ECMWF Reanalyses and Soundings, J. Climate, 14, 1823–1838, https://doi.org/10.1175/1520-0442(2001)014<1823:TCPTCD>2.0.CO;2, 2001.